TECHNICAL NOTE

A simple machine vision-driven system for measuring optokinetic reflex in small animals

**Yoshihiro Shirai · Kenta Asano ·
Yoshihiro Takegoshi · Shu Uchiyama ·
Yuki Nonobe · Toshihide Tabata**

Abstract The optokinetic reflex (OKR) is useful to monitor the function of the visual and motor nervous systems. However, OKR measurement is not open to all because dedicated commercial equipment or detailed instructions for building in-house equipment is rarely offered. Here we describe the design of an easy-to-install/use yet reliable OKR measuring system including a computer program to visually locate the pupil and a mathematical procedure to estimate the pupil azimuth from the location data. The pupil locating program was created on a low-cost machine vision development platform, whose graphical user interface allows one to compose and operate the program without programming expertise. Our system located mouse pupils at a high success rate (~ 90 %), estimated their azimuth precisely (~ 94 %), and detected changes in OKR gain due to the pharmacological modulation of the cerebellar flocculi. The system would promote behavioral assessment in physiology, pharmacology, and genetics.

Y. Shirai and K. Asano equally contributed to this work.

Y. Shirai · K. Asano · Y. Takegoshi · S. Uchiyama ·
Y. Nonobe · T. Tabata (✉)
Laboratory for Neural Information Technology, Graduate School of Sciences and Engineering, University of Toyama,
3190 Gofuku, Toyama, Toyama 930-8555, Japan
e-mail: ttabata@eng.u-toyama.ac.jp
URL: http://niteut.eng.u-toyama.ac.jp

Present Address:
Y. Shirai
Mitsubishi Electric Tokki Systems Corporation, 1-15-9 Osaki, Shinagawa-ku, Tokyo 141-0032, Japan

Keywords Eye movement · Visual system · Cerebellum · Mouse

Abbreviations

OKR   Optokinetic reflex
VBAI   Vision Builder for Automated Inspection

Introduction

The optokinetic reflex (OKR) is an ocular motion which is induced by the drift of the entire visual scene across the retina and serves to stabilize the image on the retina. Typically, an animal is exposed to an oscillating visual pattern and the stimulus-eye movement fidelity is evaluated. Such a measure efficiently quantifies the activities of the retina, accessory optic system, inferior olive, cerebellum, and vestibular and oculomotor nuclei [1–5]. OKR can be measured without ad-hoc training. Also, the basic characteristics of OKR have been documented for the mouse, a standard laboratory animal (e.g., [6, 7]). Therefore, OKR measurement is expected as a quick and informative assessment of the neural function of mutant and experimentally manipulated animals [8].

Furthermore, the fidelity increases after a long-term exposure(s) to an oscillating pattern (OKR adaptation). The analysis of OKR adaptation in mutant or experimentally manipulated mice is a powerful approach to dissecting mechanisms underlying memory formation in the cerebellar flocculus and its related brain regions (e.g., [3, 9–11]).

Despite an increasing demand for OKR measurement in small laboratory animals, there is rarely offered dedicated measurement equipment. Researchers have to build their own equipment by adapting a commercial general-purpose

eye tracker (e.g., [8, 9, 12]) or the custom equipment used in the previous studies (e.g., [6, 7, 13, 14]). However, it is difficult for non-engineer/computer expert researchers to do so because detailed instructions have not been published.

Here we describe the design of an easy-to-install/use yet reliable OKR measuring system open to all researchers. We employed machine vision, a technology used for the quality inspection of factory products, to visually locate the pupil. The computer program to execute this image processing was created on Vision Builder for Automated Inspection (VBAI) (National Instruments, TX, USA). VBAI is a machine vision-dedicated programming platform, which is much easier to manipulate than the general industrial software developing platform LabVIEW (National Instruments) whose image acquisition functionality was employed in the previously reported measurement systems [9, 14]. The cost for installing VBAI is much less expensive than LabVIEW with the machine vision-related add-ons. In the configuration mode of VBAI, one may adjust and execute the individual image processing functions like an interpreted programming language. The consequence of each adjustment can be checked instantaneously by viewing the output image of the corresponding function. These features allow intuitive and speedy optimization of the settings of the eye tracker for the examined animal. We provide the source file of the pupil locating program (VBAI diagram and its parameter settings) in Fig. 2 and supplementary material.

In addition, we describe a mathematical procedure to estimate the pupil azimuth and a sample software implementation of this procedure (supplementary material, http://niteut.eng.u-toyama.ac.jp/Lab_NIT/Downloads.html)

Fig. 2 Pupil recognition and azimuth estimation. **a–c** Online image ▶ processor which locates the pupil center. The overall state diagram (**a**) and image processing functions comprising the "Wait" (**b**) and "Inspect" (**c**) states. Screen dumps, the output images of the corresponding functions. Note that the images appear to be compressed along the y-axis because one out of two sets of interlaced scan lines were omitted from the image frame. **d–f** Off-line data analysis. The pupil rotation orbit was reconstructed, minimizing the influence of translation, re-targeting, mydriasis, and myosis and then the relative pupil azimuth (α) was determined. See "Results and discussion" and supplementary material for details

and show the performance tests of our measurement system.

Materials and methods

The detailed procedures are given in supplementary material. The animal experiments presented in this work were approved by the University of Toyama's committee on animal experiments (G-2010 ENG-16) and performed in accordance with the ethical standards laid down in the 1964 Declaration of Helsinki and the Guiding Principles for the Care and Use of Animals in the Field of Physiological Sciences. Briefly, 1 day before the measurement, a mouse was habituated to the eye tracker (Fig. 1) for ∼1 h and then dark-reared for 24 h.

One hour before the measurement, saline with or without lidocaine HCl, a local anesthetic (5 % w/v) was injected bilaterally into the cerebellar flocculi (500 nl per each side). Immediately before the measurement, the mouse was mounted on a special stereotaxic apparatus and then exposed to continuous sinusoidal oscillations of black and white stripes (Fig. 1). The infrared images of the left
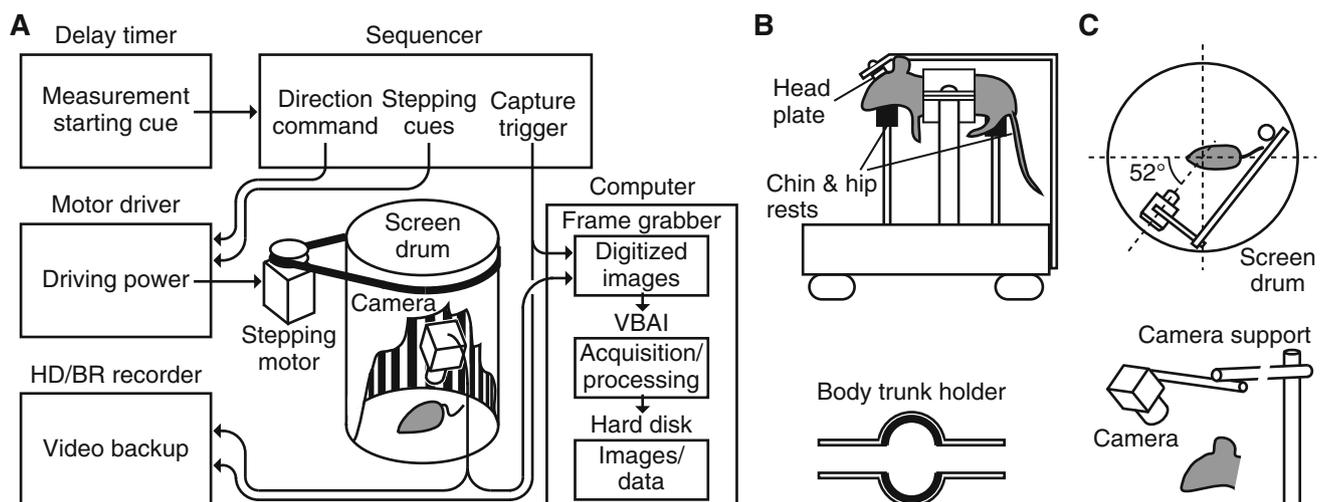
Fig. 1 Eye tracker. **a** Wiring of the devices. **b** Special stereotaxic apparatus. Black thick line, rubber lining. **c** Positioning of the camera. See supplementary material for details

A

Start

Wait

Transition 1

Inspect

Transition 2

End

B

1. Set Variable 1   →   2. Read/Write I/O

C

2. Calibrate Image

3. Detect Objects 1

1. Acquire Image →

4. Detect Objects 2

5. Threshold Image

6. Vision Assistant

7. Set Coordinate System

8. Find Edges

9. Geometry

10. Set Variable 2   →   11. Data Logging

D Translation

C_p

E Re-tracking

F Mydriasis/myosis

Pupil   Iris

r_{pupil}

Lens

Eyeball

$r_{rotation}$

$0°$

α
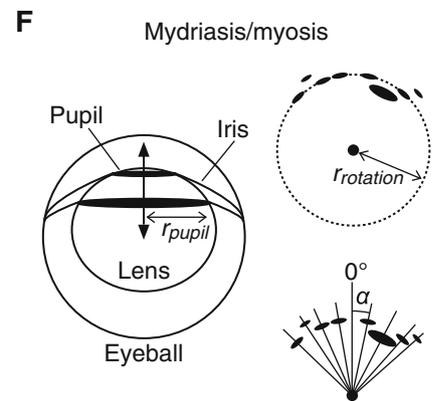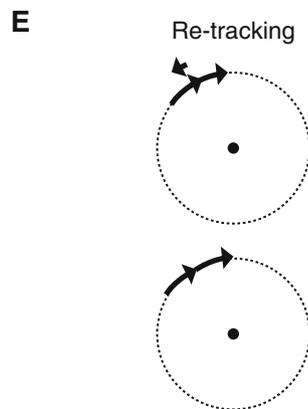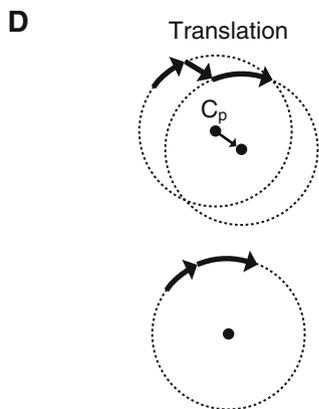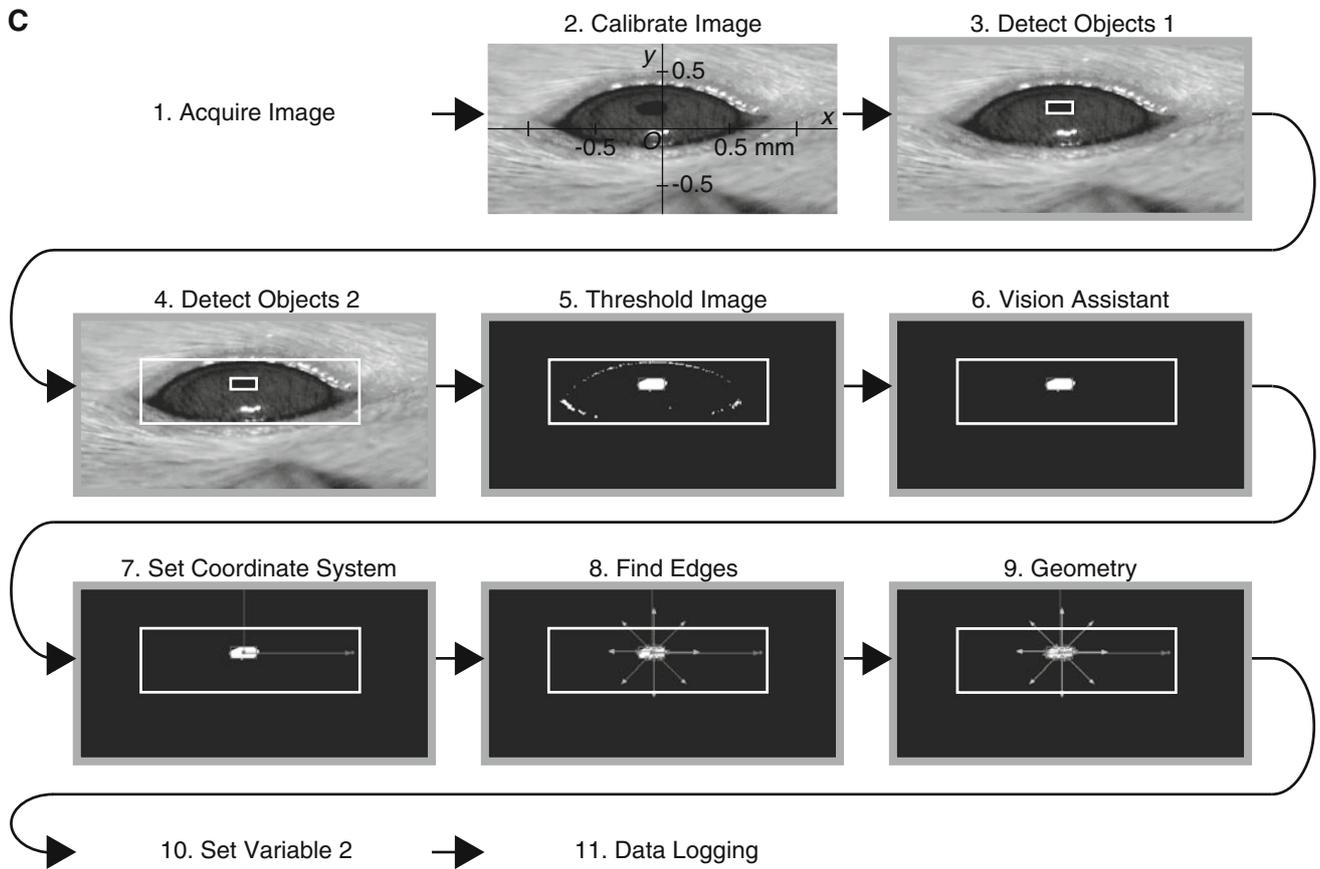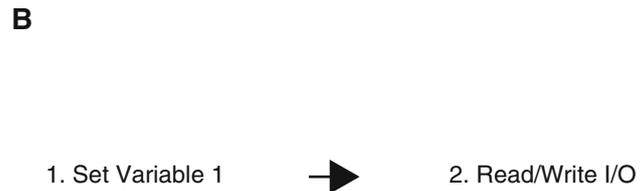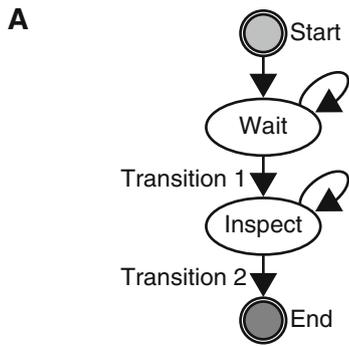
eye were captured using a charge-coupled device camera and processed using an "online image processor" software created on VBAI (version 3.6), which recognized a dark object with a certain area as the pupil and located its center by ellipse fitting (Fig. 2a–c).

After the measurement, the pupil orbit was reconstructed for every screen oscillation (Fig. 2d–f). The orbit center often moved spontaneously (translation, Fig. 2d). The eye sometimes turned in the opposite direction of the screen when the mouse switched its target from a certain group of stripes to another (re-targeting, Fig. 2e). To reduce this noise, we edited out abrupt pupil leaps from the reconstructed orbit. Moreover, mydriasis and myosis resulted in inner or outer shift of the pupil (Fig. 2f). The pupil orbit center was located by fitting a circle to the data without the indication of such a shift. Finally, relative pupil azimuth in every image frame (Fig. 2f) was determined, taking the pupil orbit center as the reference.

Results and discussion

Installation and operation

In the configuration mode of VBAI, we could compose the online image processor by graphically wiring the icons of the states and steps (built-in functions) without writing a lengthy code (Fig. 2a–c). We could also optimize the settings for the individual mouse by repeating the cycles of adjusting the parameters and checking the output image of the individual steps (Fig. 2c, supplementary material). Such an intuitive interface may allow non-computer expert researchers to build and operate the eye tracker.

Moreover, the stimulus screen drum was smoothly rotated by the stepping motor and belt pulley with a sinusoidal change in its relative azimuth (Fig. 4a, "Screen").

Basic performances

Tests with a model eye demonstrated that our system could monitor 18° rotations of the pupil with high precision (slope of the line fitted to the actual pupil azimuth-estimated pupil azimuth plot was 1.06), high linearity (R^2, 0.998), and high reproducibility (SDs, 0.034–0.356°) (Fig. 3a, b). Mice are reported to show initial OKR gains of 0.3–0.6 and a gain increases of 0.1–0.2 in response to a long-term exposure to 2–20° pattern oscillations (e.g., [3, 7, 11]; i.e., the typical amplitude of eye movement ranges 0.6–16°. Our system has enough range and resolution to evaluate OKR in mice.

Furthermore, the slope of the actual-estimated pupil azimuth plot unchanged even with translations (0.94)
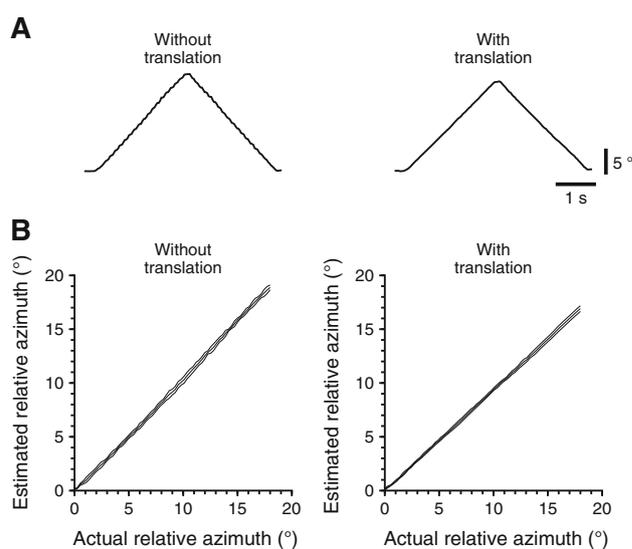
Fig. 3 Basic performances. a and b Accuracy assessment using a model eye rotating at a speed of 8.18°/s in the absence or presence of translations made by moving the model eye by ∼1 mm in random directions once every three screen oscillations. a Sample time-courses of the estimated pupil azimuth. b The relation of the actual to estimated pupil azimuth. The mean lines are flanked by the ±SD lines ($n = 5$ for each condition)

(Fig. 3b), indicating the robustness of our system against translation.

Practical performances

When applied to C57BL/6 mice, our eye tracker recognized the pupil without the indications of failure in 89.8 ± 5.8 (mean $\pm$ SD) and 87.6 ± 15.7 % of the image frames at the initial and last 10 min periods of a 1 h session, respectively ($n = 16$). If pupil recognition failed too frequently due to incorrect settings of the online image processor, we could rerun the online image processor on the backup video with the readjusted settings. Because of these fail-proof features, our system is thought to be suitable for rarely obtainable preparations such as mutant mice that are difficult to breed.

In the control mice ($n = 8$), our system could detect an increase in OKR gain (i.e., OKR adaptation) that was not seen in the lidocaine-injecected mice ($n = 6$) (Fig. 4a). There was a significant difference in the time-course of OKR gain between the control and lidocaine-injected mice ($p = 0.043$, $F = 2.46$, time × drug condition interaction, repeated measures ANOVA; Fig. 4b). In the control mice, the OKR gains at the first and last 10 min periods of a 1-h session were 0.618 ± 0.035 (mean $\pm$ SEM) and 0.714 ± 0.027, respectively. Similar time-courses and extents of OKR adaptation were reported in the previous studies [3, 11], indicating data compatibility between our and other measurement systems. In the lidocaine-injected mice, the
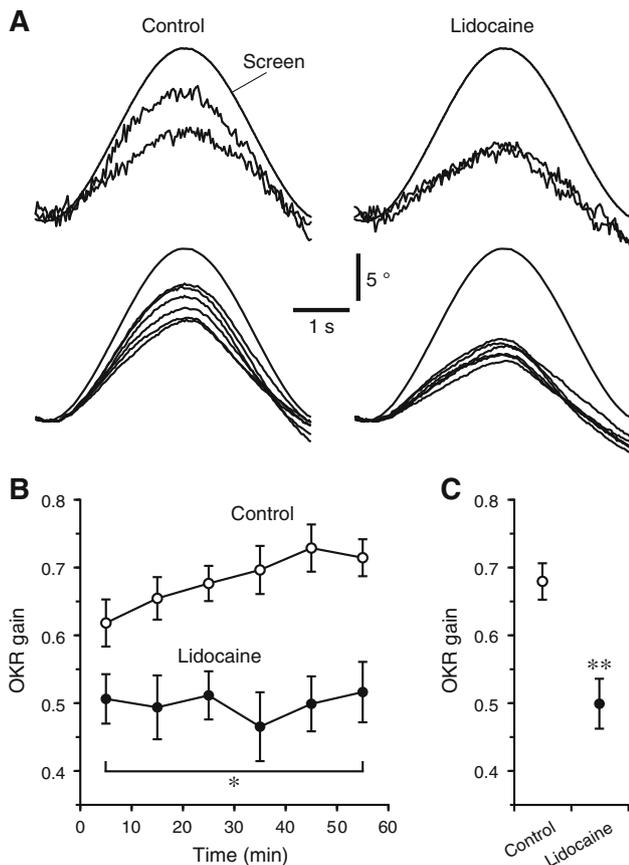
Fig. 4 Practical performances. **a–c** OKRs of the lidocaine-injected and control mice ($n = 6$ and 8, respectively). **a** Sample time-courses of the estimated pupil azimuth of single animals. Upper traces, responses to single screen oscillation obtained in the first and last 10 min periods of a 1 h measurement session. Lower traces, averages of each 10 min period of a 1 h measurement session. Screen, measured relative screen drum azimuth. **b** Average OKR gains of each 10 min period. *Dot* and *error bars*, mean ± SEM. *Asterisk*, $p = 0.043$ for time × drug condition interaction compared with the control, repeated measures ANOVA. **c** Grand mean OKR gains over the whole session. The values are calculated by averaging the data of all the 10 min periods. *Double Asterisk*, $p = 0.0015$ compared with the control, multivariate ANOVA

OKR gains at the first and last 10 min periods were 0.506 ± 0.036 and 0.516 ± 0.045, respectively. The overall OKR gains throughout the whole session also significantly differed between the control and lidocaine-injected mice ($p = 0.0015$, $F = 16.73$, multivariate ANOVA; Fig. 4c). The grand mean OKR gains over the whole session was 0.681 ± 0.027 for the control mice and 0.499 ± 0.037 for the lidocaine-injected mice. The cerebellar flocculus is thought to be responsible for formation of OKR adaptation-related memory [1, 3, 9–11]. The effect of lidocaine might reflect interference with memory formation. This result suggests that our system can evaluate the in vivo consequence of the functional modulation of the neural tissues.

Our measurement system was easy-to-install/use yet could evaluate normal and pharmacologically modulated OKRs in mice (see Additional discussion in supplementary material for details). Our system would promote behavioral examinations of mutant and experimentally manipulated small laboratory animals in physiological, pharmacological, and genetic studies.

References

1. Gittis AH, du Lac S (2006) Intrinsic and synaptic plasticity in the vestibular system. Curr Opin Neurobiol 16:385–390
2. Koekkoek SK, v Alphen AM, vd Burg J, Grosveld F, Galjart N et al (1997) Gain adaptation and phase dynamics of compensatory eye movements in mice. Genes Funct 1:175–190
3. Shutoh F, Ohki M, Kitazawa H, Itohara S, Nagao S (2006) Memory trace of motor learning shifts trans synaptically from cerebellar cortex to nuclei for consolidation. Neuroscience 139:767–777
4. Stahl JS (2004) Using eye movements to assess brain function in mice. Vision Res 44:3401–3410
5. Masseck OA, Hoffmann KP (2009) Comparative neurobiology of the optokinetic reflex. Ann N Y Acad Sci 1164:430–439
6. van Alphen AM, Stahl JS, De Zeeuw CI (2001) The dynamic characteristics of the mouse horizontal vestibulo-ocular and optokinetic response. Brain Res 890:296–305
7. Iwashita M, Kanai R, Funabiki K, Matsuda K, Hirano T (2001) Dynamic properties, interactions and adaptive modifications of vestibulo-ocular reflex and optokinetic response in mice. Neurosci Res 39:299–311
8. Cahill H, Nathans J (2008) The optokinetic reflex as a tool for quantitative analyses of nervous system function in mice: application to genetic and drug-induced variation. PLoS One 3:e2055
9. Katoh A, Kitazawa H, Itohara S, Nagao S (1998) Dynamic characteristics and adaptability of mouse vestibulo-ocular and optokinetic response eye movements and the role of the flocculo-olivary system revealed by chemical lesions. Proc Natl Acad Sci USA 95:7705–7710
10. Katoh A, Yoshida T, Himeshima Y, Mishina M, Hirano T (2005) Defective control and adaptation of reflex eye movements in mutant mice deficient in either the glutamate receptor delta2 subunit or Purkinje cells. Eur J Neurosci 21:1315–1326
11. Takeuchi T, Ohtsuki G, Yoshida T, Fukaya M, Wainai T et al (2008) Enhancement of both long-term depression induction and optokinetic response adaptation in mice lacking delphilin. PLoS One 3:e2297
12. Stahl JS, van Alphen AM, De Zeeuw CI (2000) A comparison of video and magnetic search coil recordings of mouse eye movements. J Neurosci Methods 99:101–110
13. Batini C, Ito M, Kado RT, Jastreboff PJ, Miyashita Y (1979) Interaction between the horizontal vestibulo-ocular reflex and optokinetic response in rabbits. Exp Brain Res 37:1–15
14. Sakatani T, Isa T (2004) PC-based high-speed video-oculography for measuring rapid eye movements in mice. Neurosci Res 49:123–131